PAPER

Thermo-bioconvection in stagnation point flow of third-grade nanofluid towards a stretching cylinder involving motile microorganisms

To cite this article: Taseer Muhammad *et al* 2021 *Phys. Scr.* **96** 035208

Physica Scripta

RECEIVED
6 August 2020

REVISED
5 December 2020

ACCEPTED FOR PUBLICATION
16 December 2020

PUBLISHED
29 December 2020

PAPER

Thermo-bioconvection in stagnation point flow of third-grade nanofluid towards a stretching cylinder involving motile microorganisms

Taseer Muhammad[1,*], **Malik Zaka Ullah**[2], **Hassan Waqas**[3], **Metib Alghamdi**[1] and **Arshad Riaz**[4]

[1] Department of Mathematics, College of Sciences, King Khalid University, Abha 61413, Saudi Arabia
[2] Department of Mathematics, Faculty of Science, King Abdulaziz University, Jeddah 21589, Saudi Arabia
[3] Department of Mathematics, Government College University Faisalabad, Layyah Campus 31200, Pakistan
[4] Department of Mathematics, Division of Science and Technology, University of Education, Lahore 54770, Pakistan
[*] Author to whom any correspondence should be addressed.

E-mail: tasgher@kku.edu.sa and taseer_qau@yahoo.com

Keywords: stretching cylinder, bio-convection, third grade nanofluid, arrhenius activation energy, motile microorganisms, numerical solution

Abstract

The intention of the current flow model is to investigate the significance of bioconvection in stagnation point flow of third grade nanofluid containing motile microorganisms past a radiative stretching cylinder. The impacts of activation energy and stagnation point flow are also considered. In addition the behavior of thermophoresis diffusion and Brownian motion are observed. Nanofluid can be developed by dispersing the nanosized particles into the regular fluid. Nano-sized solid materials for example carbides, grephene, metal and alloyed CNT have been utilized for the preparation of nanofluid. Physically, regular fluids have low thermal proficiency. Therefore, nano-size particles can be utilized to enhance the thermal conductivity of the host fluid. Nanofluids have many features in hybrid power engine, heat transfer, and can be used in cancer therapy and medicine. The formulated system of flow problems are transformed into dimensionless coupled ordinary differential expressions system via appropriate transformation. The systems of converted governing expressions are computed numerically by employing well known bvp4c solver in MATLAB software. The outcomes of emerging physical flow parameters on the velocity profile, volumetric concentration of then nanoparticles, rescaled density of the motile microorganisms and nanofluid temperature are elaborated graphically and numerically. Furthermore, velocity of third-grade fluid intensifies for higher values of third-grade fluid parameter and mixed convection parameter while opposite behavior is detected for buoyancy ratio parameter and mixed convection parameter. Temperature distribution grows for higher estimation of temperature ratio parameter and Biot number. Higher amount of Prandtl number and Lewis number decreases the concentration of nanoparticles. Concentration of microorganisms reduces by growing the values of velocity ratio parameter and bioconvection Lewis number.

1. Introduction

The nanofluids are fourth generation type fluid. The main elements of nano-suspension are nanoparticles in the base fluids such as water, ethylene glycol and gases. Nanoparticles are normally 1–100 nm in thickness. Nanoparticles are particularly used to improve the heat proficiency of base fluid. Nanofluids are administrating agents of drugs in dirty areas of the human body. Self-propagating drug structures are used to remove blood clots in sensitive areas such as the brain, leg, back. The essentiality of a nanofluid is due to its unique thermo physical properties. Nanofluids have significant industrial impacts. For example, electronic chip cooling, hybrid powered devices, advanced nuclear systems, photoelectric liquid heating, microchips, strong magnets and optoelectronics have attracted exceptional excitement due to their wide range of applications. In relation to the applications, the adherents investigated the effects of heat radiation on the nano-lyric flow. The thermal radiation effect may also be important if the coefficients for convective heat transfer are high. A great deal of effort has been made in recent years to improve heat efficiency and cooling. The appropriate cooling method is critical for a number of consequences, such as PCs, engines and power devices. Nanoparticles typically contains carbon annotates, oxides, metals, and carbides. Nano-fluids are useful for a wide range of applications, including heat exchangers, refrigerators, storage devices and cooling systems, nuclear reactors and computer processors. Choi [1] demonstrated the word nanoparticles inundated with normal liquids and conducted first nanofluid study. Buongiorno [2] introduced a more detailed model that includes all nanotechnology-based fluids with higher thermal properties. Alamri *et al* [3] used the Fourier Heat Flow Principle to investigate the effects of MHD on second grade fluid over stretching cylinders. Khan *et al* [4] analyzed the 2nd order slip flow impact in viscous fluid over a stretched disk. The features of hydromagnetic second order slip with nonlinear convection in nanofluid over rotating disk are scrutinized by Abbas *et al* [5]. Wang *et al* [6] discussed the three dimensional flow of Oldroyd-B nanofluid with homogeneous/heterogeneous catalytic reaction. Muhammad *et al* [7] analyzed the magnetic and electrically conducting fluid behavior over a curved surface by use entropy generation. Khan *et al* [8] scrutinized the MHD flow of casson fluid over a stretched surface in the presence of homogeneous and heterogeneous reactions. Khan and Alzahrani [9] analyzed the magneto-Jeffrey fluid over a curved surface with joule heating impacts. Hayat *et al* introduced the effect of Cattaneo-Christov heat flux and thermal conductivity in stagnation point flow of nanofluid across a variable thicked surface [10]. Further contributions on nanomaterials fluxes are found in the [11–14].

A number of non-Newtonian identities lead to investigate i.e. the mysterious natural fluid rheology. Non-Newtonian liquids are grouped into three categories i.e. differential, integral and concentrated. Third-grade liquid is used to disclose the effects of both the shear thickening phenomenon and the dilution. Third-grade mathematical model is more realistic exploration of the behavior of non-Newtonian fluids. This model also offers further study of the structure of non-Newtonian fluid flows. By earlier decades, an impact of potential applications in industry and technology third grade fluid captured the interest of several researchers. The governing equations in the third-degree fluid model are non-linear and far more complex than those for Newtonian fluids. This is worth noting. Thus, equations need more limits to provide a physically practical solution. Due to their sundry rheological properties, the nature of non-Newtonian fluids cannot be investigated by a single constituent relationship. For this liquid, there is a non-linear relationship between shear rate and shear stress. In the light of this literature review, we proposed a mathematical model for third-grade fluid flow with gyrotactic micro-organisms. This research focuses on the effects of magnetic field, thermophoresis, Brownian motion, thermal radiation and bioconvection. The Navier–Stokes model has received considerable attention in recent decades to highly non-linear fluid simulations. Ali *et al* [15] examined the effect of mixed convection fluid flow of the third grade over the stretching cylinder. Hayat *et al* [16] discussed the impacts of binary chemical reactions and activation energy on the third grade nanofluid with hydro magnetic flux with convective conditions. Chaudhuri *et al* [17] investigated thermal transfer properties of magnetohydrodynamic (MHD) that is subjected to a uniform thermal flux in the wall, but of varying magnitudes, of a third-grade fluid between parallel plates. Hayat *et al* [18] explore the characteristics of a magnetohydrodynamic third-grade nanofluid with triggering energy and binary chemical reactions. Alzahrani *et al* [19] discussed the magnetohydrodynamic, third-grade fluid flow with gyrotactic microorganisms across a horizontal porous extension sheet. Okoya *et al* [20] analyzed the mass and heat transfer numerically by using a fixed cylindrical annulus to neglect the material consumption in a pressure-induced third-grade reactive fluid with the Reynolds Viscosity Model. Sajid *et al* [21] explored process of coating a third grade liquid to a moving substrate using a flat, fixed blade is described. Mahanthesh *et al* [22] worked on Non-transient dynamics in the presence of non-Newtonian third-grade pressure-driven nanoparticles. Golafshan *et al* [23] examined the issue of a non-Newtonian magnetohydrodynamic nanomaterial, confined by a vertical stretching sheet, to be a two dimensional mixed stagnation-flow of convection.

Stagnation point flow was observed by many researchers and scientists due to its broad application in industries for example hot rolling, paper making. In 1911, Hiemens [24] analyzed the stagnation point flow. Sajjad *et al* [25] explored the stagnation point flow of second grade nanofluid past a stretching surface. Ghasemian *et al* [26] analyzed the stagnation point flow of Maxwell nanofluid over a cylinder.

Nanofluids containing gyrotactic microorganisms are used to improve fluid mixing because they are responsible for the bioconvection process. Such species are denser than water, and normally move in the direction of the atmosphere. Bioconvection is a mechanical process that is quite attractive to the space. In low suspensions of upward-swimming cells (against gravity), a change of attitude is noted. It also affects the spatial distribution of transportable microorganisms in marine settings and promotes mixing of the fluids. Microorganisms are single cell organisms as they occur in plants, humans, and insects. Bioconvection causes microorganisms because they are much denser than water due to aggregation of microorganisms. Bioconvection caused by the density differences of motile microorganisms is effectively assorted in the field of environmental systems, biofuels, and industry. Immunology Microsystems (i.e., biomaterials, tissue engineering, protein engineering, synthetic biology, and drug delivery systems) such as enzyme biosensors are typically involved in bioconvection applications.

Khan *et al* [27] elaborated the natural boundary convection flow of water based nanofluid consisting of gyrotactic motile microorganisms on a truncated surface cone. Rashad *et al* [28] described bioconvection of nanofluids made up of gyrotactic motile microorganisms that is subjected to a horizontal circular cylinder with convective boundary restrictions. Naz *et al* [29] demonstrated the dynamic engineering of nanofluid in the magnetohydrodynamic circle, including gyrotactic microorganisms. Al-Khaled *et al* [30] studied the theoretical work which deals with the application of the bioconvection phenomenon on tangent hyperbolic nanofluid motion over an accelerated moving surface. Waqas *et al* [31] divulged the impact of bioconvection of nanofluids has been problematic over the last decades because it has a wide range of physical significance in biotechnology. Balla *et al* [32] studied the bioconvective flow in the presence of a chemical reaction in a porous square cavity containing an oxytactic microorganism. Naganthran *et al* [33] reported that bioconvection nanofluid transport is a new focal point for fluid dynamics, as suspensions of microorganisms and nanoparticles have shown to enhance their thermal conductivity, such as biofuels cells and bio-micro fluid systems that support many industrial applications. Zuhra *et al* [34] developed the mathematical model for the analysis of the simultaneous flow of two Nanoliquids (Casson and Williamson) through a porous medium under the influence of boom forces, in presence of cubic-autocatalysis chemical reactions and motile microorganisms. Mansour *et al* [35] numerically studied magnetohydrodynamic mixed convection with gyrotactic micro-organisms in a carriage-driven cavity. Zeng *et al* [36] studied that continuum model for horizontal change diluted suspension, with a maximum number of Reynolds up to 100, past a single, solid, longitudinal, circular ring stretching from a flat horizontal bed to a free water surface, as a first step towards understanding the spread of swimming microorganisms in shallow water flow with vegetation. Khan *et al* [37] explored the brief overview of the boundary layer flow characterizing magnetically modified Newtonian fluids caused by the transformation of the bioconvection parabolic and chemical reactive species is described. Mallikarjuna *et al* [38] examined the nanofluid flow containing gyrotactic microorganisms in a continuous mixing of bioconvection through a thin vertical channel. Waqas *et al* [39] scrutinized modified second grade nanofluid flow with heat, motile microorganisms and mass transfer through the stretching surface. Waqas *et al* [40] discussed the thermal and mass transfer phenomenon in the presence of a motile gyrotactic microorganism in the presence of Williamson's time-based magnetohydrodynamic (MHD) flow. Khan *et al* [41] explored theoretical continuation of couple stress nanofluid, under porous media, gyrotactic microorganisms, activation energy and convective conditions to meet present challenges in processing of nano-biomatogens and improving thermal extrusion systems. Ray *et al* [42] analyzed the numerically a thin electrical conductive film of Newtonian Casson with even width on a horizontal elastic sheet resulting from a slit in the presence of viscous dissipation, a two-dimensional, unstable, magnetohydrodynamic bioconvection flow. Amirsom *et al* [43] illustrated three-dimensional bioconvection flow with gyrotactic microorganisms over a biaxial stretching sheet was suggested for theoretical analysis. Al-Kaled *et al* [30] examines the application of the biological convection effect to the accelerated moving surface of the tangent hyperbolic nanofluid. Khan *et al* [44] scrutinized the impact of thixotropic nanofluids on nonlinear mixed convective flow. Naz *et al* [45] explored nanofluid research carried out by Walters B fluid under the influence of Joule heating and magnets flowing through horizontal cylindrical surfaces; viscous dissipation, microorganisms swimming and stratification. Chakraborty *et al* [46] investigate the combined effect of nanofluid flow on bioconvection along the expansion sheet coexisting with gyrotactic magnetic field microorganisms and the convective boundary conditions. Khan *et al* [47] analyzed the effect of microorganisms in Walter-B fluid towards a stretched surface.

The novelty of this analysis is to explore the stagnation point flow of radiative-third grade fluid containing gyrotactic motile microorganisms over a stretching cylinder in the presence of bioconvection phenomenon. In current investigation nonlinear mathematical model featuring third grade nanofluid is developed. Famous shooting scheme is used to treat the system of ordinary differential equations. Furthermore bvp4c collocation method is used for simulation. The current problem has many applications in real world in nanotechnology, electrical and mechanical engineering, biotechnology and biomedicine and industries. These type problems are more useful in high nuclear systems, chemical sciences, drug delivery, cancer therapy, crystal growthing and military fields.

2. Mathematical model

Here, the stagnation point flow of third grade nanofluid with motile microorganisms past a radiative stretching cylinder is scrutinized. The significance of activation energy, thermal radiation, and Brownian motion, thermophoresis aspects is accounted. Let us consider velocity of the stretching cylinder $W_w(z) = \frac{W_0 z}{l}$ directed along z-direction, where z is velocity reference and specific length l. The cylindrical polar coordinates $(\breve{r}, \breve{z})$ are

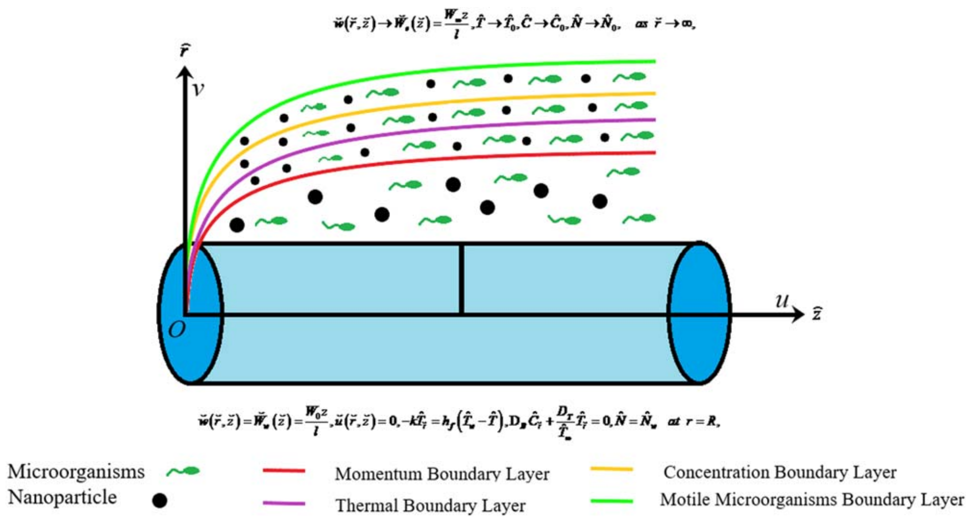

Figure 1. Flow configuration of current model.

chosen, in such direction, z-axis along cylinder while r-axis is orthogonal to it. The velocity components $\breve{u}$, $\breve{w}$) are specified in ($\breve{r}$, $\breve{z}$) way. The uniform magnetic field of strength B_0 is applied due to poorer magnetic Reynolds number the electric and induced magnetic field are ignored. Physical flow configuration of the current model in the absence of porous medium is depicted in figure 1.

$$\breve{u}_{\breve{r}} + \frac{\breve{u}}{\breve{r}} + \breve{w}_{\breve{z}} = 0, \tag{1}$$

$$\begin{aligned}
\rho_f(\breve{u}\breve{w}_{\breve{r}} + \breve{w}\breve{w}_{\breve{z}}) = {} & W_e\frac{d\breve{W}_e}{d\breve{z}} + \mu\left(\breve{w}_{\breve{r}\breve{r}} + \frac{1}{\breve{r}}\breve{w}_{\breve{r}}\right) + \frac{\sigma B_0^2}{\rho_f}(-\breve{w} - \alpha_1\breve{w}_{\breve{r}}) \\
& + \alpha_1\begin{bmatrix} \frac{\breve{w}}{\breve{r}}\breve{w}_{\breve{r}\breve{z}} + \frac{\breve{u}}{\breve{r}}\breve{w}_{\breve{r}\breve{r}} + \frac{3}{\breve{r}}\breve{w}_{\breve{r}}\breve{w}_{\breve{z}} + \frac{1}{\breve{r}}\tilde{u}_{\breve{r}}\breve{w}_{\breve{r}} \\ +4\breve{w}_{\breve{r}}\breve{w}_{\breve{r}\breve{z}} + \breve{w}\breve{w}_{\breve{r}\breve{r}\breve{z}} + 2\breve{u}_{\breve{r}}\breve{w}_{\breve{r}\breve{r}} + \breve{u}\breve{w}_{\breve{r}\breve{r}\breve{r}} \\ +3\breve{w}_{\breve{r}\breve{r}}\breve{w}_{\breve{z}} + \breve{u}_{\breve{r}\breve{r}}\frac{\partial^2 u}{\partial r^2}\frac{\partial w}{\partial r} \end{bmatrix} \\
& + \alpha_2\begin{bmatrix} \frac{2}{\breve{r}}\breve{u}_{\breve{r}}\breve{w}_{\breve{r}} + \frac{2}{\breve{r}}\breve{w}_{\breve{r}}\breve{w}_{\breve{z}} + 2\breve{w}_{\breve{r}\breve{r}}\breve{w}_{\breve{r}} + 2\breve{u}_{\breve{r}}\breve{w}_{\breve{r}\breve{r}} \\ +2\breve{w}_{\breve{r}\breve{r}}\breve{w}_{\breve{z}} + 4\breve{w}_{\breve{r}}\breve{w}_{\breve{r}\breve{z}} \end{bmatrix} \\
& + \beta_3\left[\frac{2}{\breve{r}}(\breve{w}_{\breve{r}})^3 + 6(\breve{w}_{\breve{r}})^2\breve{w}_{\breve{r}\breve{r}}\right] \\
& + \frac{1}{\rho_f}\begin{bmatrix} (1 - \hat{C}_f)\rho_f\beta^{**}g^*(\hat{T} - \hat{T}_\infty) - (\rho_p - \rho_f)g^*(\hat{C} - \hat{C}_\infty) \\ -(\hat{N} - \hat{N}_\infty)g^*\gamma^*(\hat{\rho}_m - \hat{\rho}_f) \end{bmatrix},
\end{aligned} \tag{2}$$

$$\begin{aligned}
\breve{u}\hat{T}_{\breve{r}} + \breve{w}\hat{T}_{\breve{z}} = {} & \frac{k}{\rho c_p}\left(\hat{T}_{\breve{r}\breve{r}} + \frac{1}{\breve{r}}\hat{T}_{\breve{r}}\right)\frac{1}{r(\rho c)_f}\left(\frac{r}{\Delta T}(\hat{T} - \hat{T}_\infty)\hat{T}_{\breve{r}}\right)_{\breve{r}} + \tau\left[D_B\hat{C}_{\breve{r}}\hat{T}_{\breve{r}} + \frac{D_T}{\hat{T}_\infty}(\hat{T}_{\breve{r}})^2\right] \\
& + \frac{16\sigma\hat{T}_\infty^3}{3k^*\rho c_p}\left(\hat{T}_{\breve{r}\breve{r}} + \frac{1}{\breve{r}}\hat{T}_{\breve{r}}\right) + \frac{Q_0}{(\rho c)_f}(\hat{T} - \hat{T}_\infty),
\end{aligned} \tag{3}$$

$$\breve{u}\hat{C}_{\breve{r}} + \breve{w}\hat{C}_{\breve{z}} = D_B\left(\hat{C}_{\breve{r}\breve{r}} + \frac{1}{\breve{r}}\hat{C}_{\breve{r}}\right) + \frac{D_T}{\hat{T}_\infty}\left[\hat{T}_{\breve{r}\breve{r}} + \frac{1}{\breve{r}}\hat{T}_{\breve{r}}\right] - Kr^2(\hat{C} - \hat{C}_\infty)\left(\frac{\hat{T}}{\hat{T}_\infty}\right)^n\exp\left(\frac{-E_a}{k\hat{T}}\right), \tag{4}$$

$$\breve{u}\hat{N}_{\breve{r}} + \breve{w}\hat{N}_{\breve{z}} + \left[\frac{\hat{N}}{\breve{r}}\hat{C}_{\breve{r}} + +\hat{N}_{\breve{r}}\hat{C}_{\breve{r}} + \hat{N}\hat{C}_{\breve{r}\breve{r}}\right]\frac{bW_c}{(\hat{C}_w - \hat{C}_0)} = D_m\left(\hat{N}_{\breve{r}\breve{r}} + \frac{1}{\breve{r}}\hat{N}_{\breve{r}}\right), \tag{5}$$

Boundary restrictions are as follows:

$$\breve{w}(\breve{r},\breve{z}) = \breve{W}_w(\breve{z}) = \frac{W_0 z}{l},\ \breve{u}(\breve{r},\breve{z}) = 0,\ -k\hat{T}_{\breve{r}} = h_f(\hat{T}_w - \hat{T}),\ D_B\hat{C}_{\breve{r}} + \frac{D_T}{\hat{T}_\infty}\hat{T}_{\breve{r}} = 0,$$
$$\hat{N} = \hat{N}_w\ at\ r = R, \tag{6}$$

$$\breve{w}(\breve{r},\breve{z}) \to \breve{W}_e(\breve{z}) = \frac{W_\infty z}{l},\ \hat{T} \to \hat{T}_0,\ \hat{C} \to \hat{C}_0,\ \hat{N} \to \hat{N}_0,\ as\ \breve{r} \to \infty, \tag{7}$$

Where radial distance is $\breve{r}$ while $\breve{z}$ axial distance, $\breve{u}$, $\breve{w}$ fluid velocity, α_1, α_2 and β_3 represents the third grade variables, ρ_f density of nanofluid, $\hat{T}_w$, $\hat{C}_w$ and $\hat{N}_w$ are surface temperature, surface concentration and surface concentration of microorganisms respectively, heat source/sink constant Q_0, D_B stand for Brownian motion diffusion constant, D_m microorganisms diffusion constant, D_T is thermophoresis diffusion constant, Kr^2 reaction rate constant, fitted rate constant n, chemotaxis constant represent as b, c_p heat capacity of nanofluid, ρ_p is density of nanoparticles and W_c is maximum cell swimming speed.

The appropriate transformations

$$\breve{w}(\breve{r},\breve{z}) = \frac{W_0 z}{l} f'(\zeta),\ \breve{u}(\breve{r},\breve{z}) = -\sqrt{\frac{\nu W_0}{l}}\frac{R}{r} f(\zeta),\ \ \zeta = \sqrt{\frac{W_0}{\nu l}}\left(\frac{r^2 - R^2}{2R}\right),$$
$$\theta(\zeta) = \frac{\hat{T} - \hat{T}_\infty}{\hat{T}_w - \hat{T}_0},\ \ \phi(\zeta) = \frac{\hat{C} - \hat{C}_\infty}{\hat{C}_w - \hat{C}_0},\ \ \chi(\zeta) = \frac{\hat{N} - \hat{N}_\infty}{\hat{N}_w - \hat{N}_0}, \tag{8}$$

By employingsimilaritiestransformations (8) then expressions (1)–(7) are

$$\begin{aligned}
&(1 + 2\gamma\zeta)\frac{d^3f}{d\zeta^3} + B^2 + 2\gamma\frac{d^2f}{d\zeta^2} - \left(\frac{df}{d\zeta}\right)^2 + f\frac{d^2f}{d\zeta^2} - M^2\left(\frac{df}{d\zeta} - \beta_1 f\frac{d^2f}{d\zeta^2}\right)\\
&+ \beta_1\left[(1 + 2\gamma\zeta)\left\{2\frac{df}{d\zeta}\frac{d^3f}{d\zeta^3} - f\frac{d^4f}{d\zeta^4} + 3\left(\frac{d^2f}{d\zeta^2}\right)^2\right\} + \gamma\left(6\frac{df}{d\zeta}\frac{d^2f}{d\zeta^2} - 2f\frac{d^3f}{d\zeta^3}\right)\right]\\
&+ \beta_2\left[2(1 + 2\gamma\zeta)\left(\frac{d^2f}{d\zeta^2}\right)^2 + \gamma\left(2\frac{df}{d\zeta}\frac{d^2f}{d\zeta^2} + 2f\frac{d^3f}{d\zeta^3}\right)\right]\\
&+ \alpha R_e\left[6(1 + 2\gamma\zeta)^2\left(\frac{d^2f}{d\zeta^2}\right)^2\frac{d^3f}{d\zeta^3} + 8\gamma(1 + 2\gamma\zeta)\left(\frac{d^2f}{d\zeta^2}\right)^3\right]\\
&+ \lambda(\theta - Nr\phi - Nc\chi)\ = 0\ ,
\end{aligned} \tag{9}$$

Where $\gamma = \sqrt{\left(\frac{\nu l}{W_0 R^2},\right)}$ is curvature parameter, $\beta_1 = \frac{\alpha_1^* W_0}{l\mu}$, $\beta_2 = \frac{\alpha_2^* W_0}{l\mu}$, and $\alpha = \frac{\beta_3 W_0^2}{l^2\mu}$ are third grade fluid parameters, Reynolds number $\mathrm{Re} = \frac{Wz}{\nu}$, mixed convection parameter expressed as $\lambda = \frac{l^2\beta^{**}g^*(1 - \hat{C}_\infty)(\hat{T}_w - \hat{T}_0)}{zW_0^2\rho_f}$, magnetic parameter $M = \frac{\sigma B_0^2 l}{W_0\rho_f}$, $Nr = \frac{(\rho_p - \rho_f)(\hat{C}_w - \hat{C}_o)}{(1 - \hat{C}_\infty)(\hat{T}_w - \hat{T}_0)}$ stand for buoyancy ratio parameter and bioconvection Rayleigh number is $Nc = \frac{\gamma^*(\rho_m - \rho_f)(\hat{N}_w - \hat{N}_0)}{(1 - \hat{C}_\infty)(\hat{T}_w - \hat{T}_0)\beta^{**}}$.

$$\begin{aligned}
&\left(1 + \frac{4}{3}Rd\right)(1 + 2\gamma\zeta)\frac{d^2\theta}{d\zeta^2} + 2\gamma\left(1 + \frac{4}{3}Rd\right)\frac{d\theta}{d\zeta} + \mathrm{Pr}\left(f\frac{d\theta}{d\zeta} - \frac{df}{d\zeta}\theta\right)\\
&+ \frac{2}{3Rd}\left[\{1 + (\theta_f - 1)\theta\}^3\left(2\gamma\frac{d\theta}{d\zeta} + 2\frac{d^2\theta}{d\zeta^2}(1 + 2\gamma\zeta)\right) + 6\{1 + (\theta_f - 1)\theta\}^2\right]\\
&+ (1 + 2\gamma\zeta)\mathrm{Pr}Nb\frac{d\theta}{d\zeta}\frac{d\phi}{d\zeta} + (1 + 2\gamma\zeta)\mathrm{Pr}Nt\left(\frac{d\theta}{d\zeta}\right)^2 + Q\theta = 0,
\end{aligned} \tag{10}$$

Where $Rd = \frac{4\sigma^* T_\infty^3}{k^* k}$ stand for Radiation parameter, Prandtl number $Pr = \frac{\nu}{\alpha}$ is Prandtl number, Brownian motion parameter $Nb = \frac{\tau(\hat{C}_w - \hat{C}_0)}{\nu}D_B$, thermophoresis parameter $Nt = \frac{\tau(\hat{T}_w - \hat{T}_0)D_T}{\hat{T}_\infty\nu}$, temperature ratio parameter is $\theta_f = \frac{\hat{T}_w}{\hat{T}_\infty}$ and Heat source/sink parameter $Q = \frac{lQ_0}{W_0(\rho c)_f}$.

$$(1+2\gamma\zeta)\frac{d^2\phi}{d\zeta^2}+2\gamma\frac{d\phi}{d\zeta}+Le\Pr\left(f\frac{d\phi}{d\zeta}-\frac{df}{d\zeta}\phi\right)+(1+2\gamma\zeta)\left(\frac{Nt}{Nb}\right)\frac{d^2\theta}{d\zeta^2}$$
$$+2\gamma\left(\frac{Nt}{Nb}\right)\frac{d\theta}{d\zeta}-\Pr Le\sigma^*(1+\delta\theta)^n\exp\left(\frac{-E}{(1+\delta\theta)}\right)\phi=0, \tag{11}$$

Where Lewis number is $Le=\frac{\alpha}{D_B}$, chemical reaction parameter is $\sigma^*=\frac{lKr^2}{W_0}$, temperature difference parameter denoted by $\delta=\frac{\hat{T}_w-\hat{T}_0}{\hat{T}_\infty}$, $E=\frac{E_a}{k\hat{T}}$ stand for activation energy.

$$(1+2\gamma\zeta)\frac{d^2\chi}{d\zeta^2}+2\gamma\frac{d\chi}{d\zeta}-Lb\chi\frac{df}{d\zeta}+Lbf\frac{d\chi}{d\zeta}$$
$$-Pe\left(\left(\frac{d^2\phi}{d\zeta^2}(1+2\gamma\zeta)+2\gamma\frac{d\phi}{d\zeta}\right)(\chi+\delta_1)+(1+2\gamma\zeta)\frac{d\chi}{d\zeta}\frac{d\phi}{d\zeta}\right)=0, \tag{12}$$

Here bioconvection Lewis number is $Lb=\frac{\nu}{D_m}$, Peclet number is $Pe=\frac{bW_c}{D_m}$, microorganism's and difference parameter $\delta_1=\frac{\hat{N}_\infty}{\hat{N}_w-\hat{N}_0}$.

With

$$\frac{df}{d\zeta}(0)=1,\ f(0)=0,\ \frac{df}{d\zeta}(\infty)=B, \tag{13}$$

$$\frac{d\theta}{d\zeta}(0)=-Bi(1-\theta(0)),\ \ \theta(\infty)\to 0, \tag{14}$$

$$Nb\frac{d\phi}{d\zeta}+Nt\frac{d\theta}{d\zeta}=0,\ \ \phi(\infty)\to 0, \tag{15}$$

$$\chi(0)=1,\ \ \chi(\infty)\to 0, \tag{16}$$

Where $Bi=\frac{h_f}{k}\sqrt{\frac{\nu l}{W_0}}$ stand for Biot number. The engineering variables namely local Sherwood number, local Nusselt number and local density number of motile microorganisms are expressed as

$$Nu_z=\frac{zq_m}{k(\hat{T}_w-\hat{T}_0)},\ sh_z=\frac{zh_w}{D_B(\hat{C}_w-\hat{C}_0)},\ Nn_z=\frac{zq_n}{D_m(\hat{N}_w-\hat{N}_0)}$$
$$where\ q_m=-k(\hat{T}_{\check{r}}),\ h_w=-D_B(\hat{C}_{\check{r}})_{r=R'},\ \mathrm{q}_n=-D_m(\hat{N}_{\check{r}})_{r=R} \tag{17}$$

The dimensionless form of expression (16)

$$\mathrm{Re}_z^{-1/2}C_f=\left[1+3\alpha_1+3\beta\,\mathrm{Re}\left(\frac{d^2f}{d\zeta^2}(0)\right)^2\right]\frac{d^2f}{d\zeta^2}(0), \tag{18}$$

$$Nu_z\,\mathrm{Re}_z^{-1/2}=-\left(1+\frac{4}{3}Rd\right)\frac{d\theta}{d\zeta}(0), \tag{19}$$

$$Sh_z\,\mathrm{Re}_z^{-1/2}=-\frac{d\phi}{d\zeta}(0), \tag{20}$$

$$Nn_z\,\mathrm{Re}_z^{-1/2}=-\frac{d\chi}{d\zeta}(0), \tag{21}$$

Here $\mathrm{Re}_z=W_w\frac{l}{\nu}$ is local Reynolds number.

3. Numerical procedure

In this segmentation, the dimensionless nonlinear expressions (9)–(12) subject to the boundary conditions (13)–(16) are tackled numerically. It's hard to find exact solution because equations are highly nonlinear in feature. We employ a well-known numerical scheme bvp4c shooting method is followed for suitable numerical calculation throughout the MATLAB software. Before starting process, the system of higher order ODEs are converted into first order ordinary differential equations by introducing interesting variables.

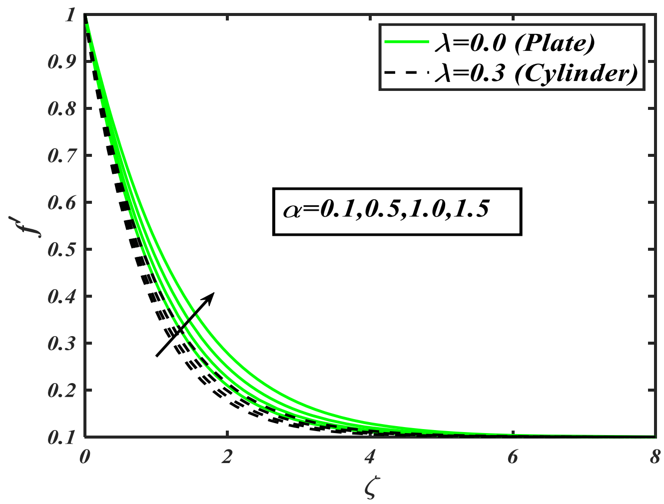

Figure 2. Sketch of f' against α.

Let

$$\begin{aligned} &f = r_1,\ \frac{df}{d\zeta} = r_2,\ \frac{d^2f}{d\zeta^2} = r_3,\ \frac{d^3f}{d\zeta^3} = r_4,\ \frac{d^4f}{d\zeta^4} = r_4',\\ &\theta = r_5,\ \frac{d\theta}{d\zeta} = r_6,\ \frac{d^2\theta}{d\zeta^2} = r_6',\\ &\phi = r_7,\ \frac{d\phi}{d\zeta} = r_8,\ \frac{d^2\phi}{d\zeta^2} = r_8',\\ &\chi = r_9,\ \frac{d\chi}{d\zeta} = r_{10},\ \frac{d^2\chi}{d\zeta^2} = r_{10}', \end{aligned} \tag{22}$$

$$\begin{aligned} r_4' = &\frac{1}{\beta_1 r_1(1+2\gamma\zeta)}[(1+2\gamma\zeta)r_4 - r_2^2 + B^2 + 2\gamma r_3 + r_1 r_3]\\ &+\frac{1}{\beta_1 r_1(1+2\gamma\zeta)}\langle\beta_1[(1+2\gamma\zeta)\{2r_2r_4 + 3r_3^2\} + \gamma(6r_2r_3 - 2r_1r_4)]\rangle\\ &+\frac{1}{\beta_1 r_1(1+2\gamma\zeta)}\langle\beta_2[2(1+2\gamma\zeta)r_3^2 + \gamma(2r_2r_3 + 2r_1r_4)]\rangle\\ &+\frac{1}{\beta_1 r_1(1+2\gamma\zeta)}\langle\alpha Re[6(1+2\gamma\zeta)^2 r_3^2 r_4 + 8\gamma(1+2\gamma\zeta)r_3^3]\rangle\\ &+\frac{1}{\beta_1 r_1(1+2\gamma\zeta)}[r_2 - \beta_1 r_1 r_3] - \frac{1}{\beta_1 r_1(1+2\gamma\zeta)}\langle\lambda(r_5 - Nrr_7 - Ncr_9)\rangle, \end{aligned} \tag{23}$$

$$r_6' = \frac{\begin{bmatrix} \Pr(r_2r_5 + r_2r_5) - 2\gamma\left(1+\frac{4}{3}Rd\right)r_6 - (1+2\gamma\zeta)\Pr Nbr_6r_8 - (1+2\gamma\zeta)\Pr Ntr_6^2 - Qr_5\\ -\frac{2}{3Rd}[\{1+(\theta_f-1)r_5\}^3(2\gamma r_6) + 6\{1+(\theta_f-1)r_5\}^2] \end{bmatrix}}{\left(1+\frac{4}{3}Rd\right)\frac{2}{3Rd}((1+\theta_f-1)r_5)^3(1+2\gamma\eta)}, \tag{24}$$

$$r_8' = \frac{1}{(1+2\gamma\zeta)}\begin{bmatrix} -2\gamma r_8 - (1+2\gamma\zeta)\frac{Nt}{Nb}r'_6 - 2\gamma\frac{Nt}{Nb}r_6 - LePr(r_1r_8 - r_2r_7)\\ +\Pr Le\sigma^*(1+\delta r_5)^n\exp\left(\frac{-E}{1+\delta r_5}\right)r_7 \end{bmatrix}, \tag{25}$$

$$\begin{aligned} r_{10}' = &-2\gamma r_{10} + Pe[(r_9+\delta_1)(2\gamma r_8 + (1+2\gamma\zeta)r'_8) + (1+2\gamma\zeta)r_{10}r_8]\\ &+ Lbr_9r_2 - Lbr_1r_{10}, \end{aligned} \tag{26}$$

With

$$\begin{aligned} &r_2(0) = 1,\ r_1(0) = 0,\ r_5(0) = 1,\ r_6(0) = -Bi(1 - r_5(0)),\ Nbr_8 + Ntr_6 = 0,\ r_9(0) = 1,\\ &r_2(\infty) = B,\ r_5(\infty) \to 0,\ r_7(\infty) \to 0,\ r_9(\infty) \to 0, \end{aligned} \tag{27}$$

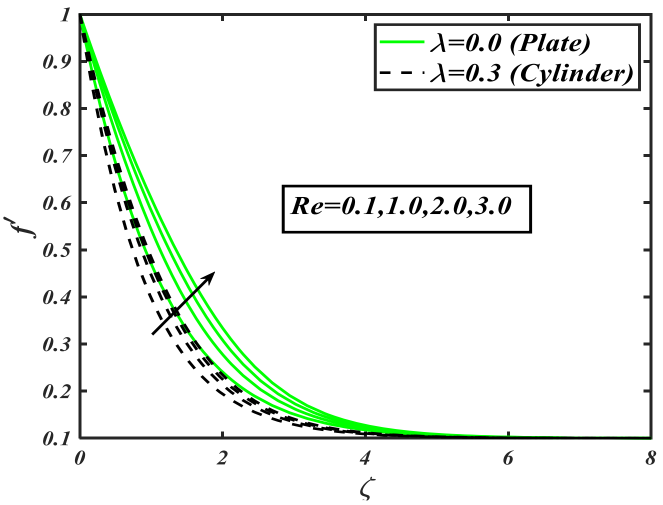

Figure 3. Sketch of f' against Re.

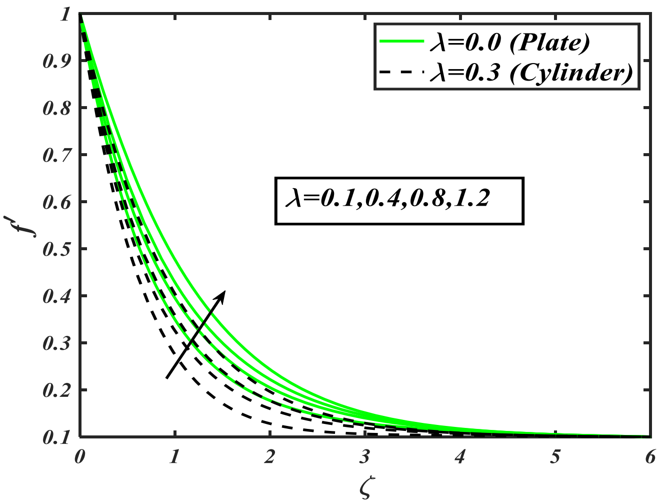

Figure 4. Sketch of f' against λ.

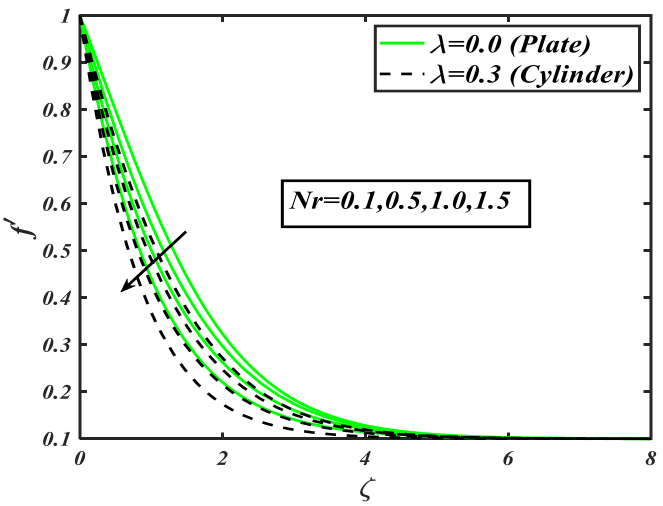

Figure 5. Sketch of f' against Nr.

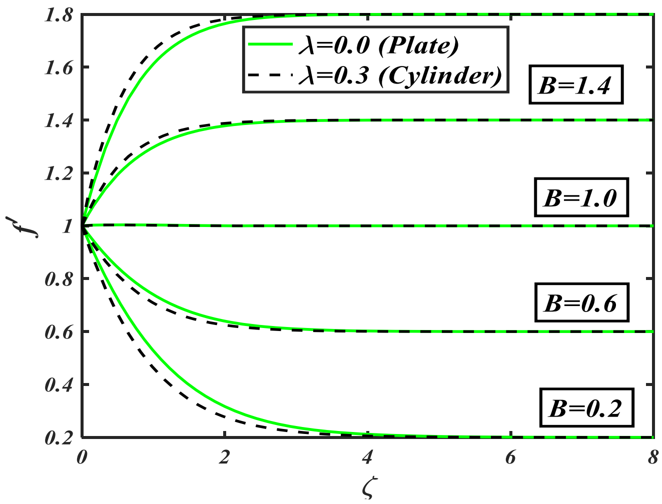

Figure 6. Sketch of f' against B.

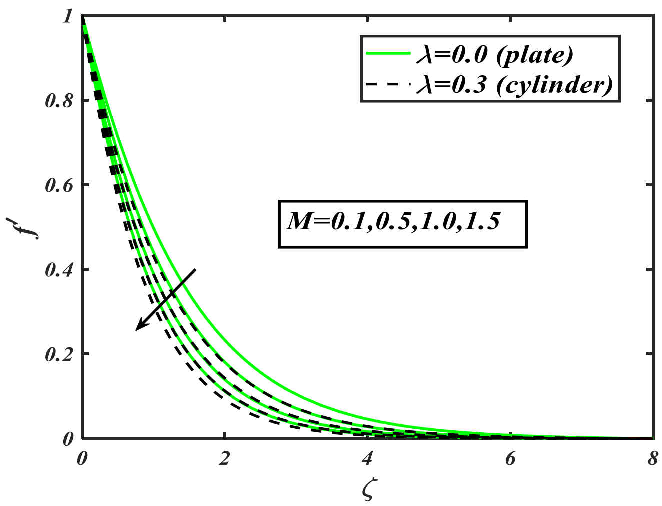

Figure 7. Sketch of f' against M.

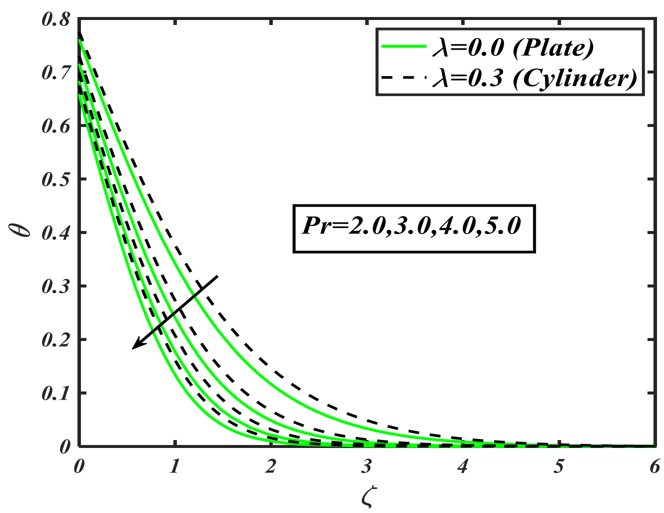

Figure 8. Sketch of θ against Pr.

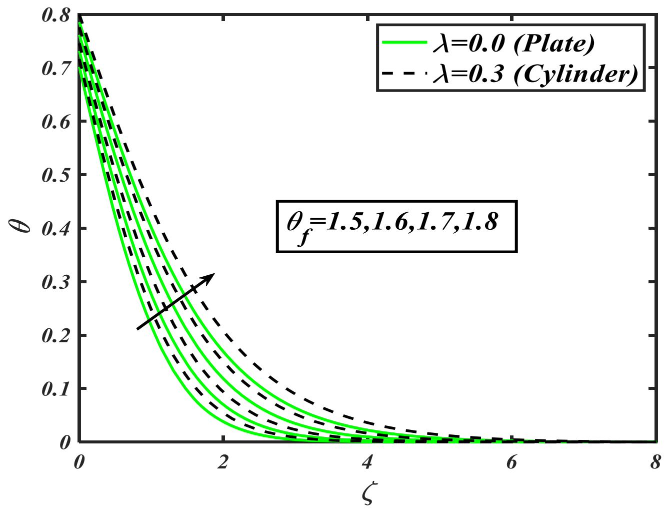

Figure 9. Sketch of θ against θ_f.

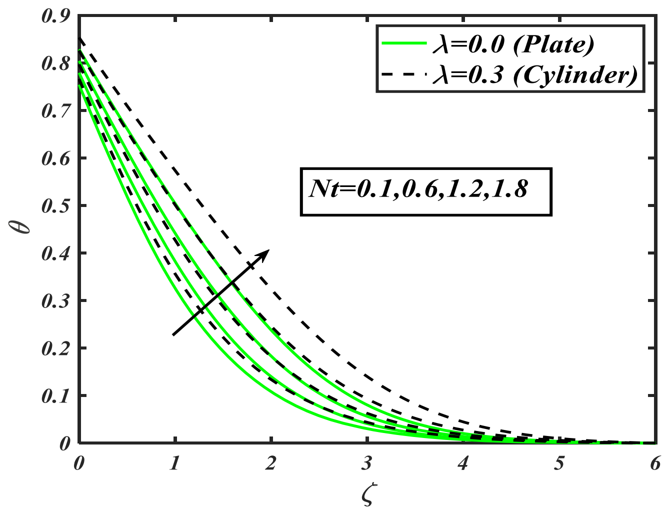

Figure 10. Sketch of θ against Nt.

4. Results and discussion

This portion is concerned with significant features of prominent variables on velocity; temperature, nanoparticles concentration and motile microorganism concentration are disclosed and graphically captured.

Figure 2 is captured to depicting the behavior of third grade fluid α on velocity f'. Velocity profile f' enhance for higher value of third grade fluid number α. Figure 3 is plotted to observe the features of Reynolds Re on velocity f'. For higher values of Reynolds Re the velocity f' enhancing. The variations of velocity field f' versus mixed convection parameter λ are validated in figure 4. The growing aspect in velocity profile f' is observed in figure 4. Figure 5 is captured to focus the features on velocity field f' set up by buoyancy ratio parameter Nr. The fact that buoyancy ratio parameter Nr has a reducing behavior on the velocity field f' is shown in figure 5. Behavior of velocity ratio parameter B on velocity profile f' is studied in figure 6. It is noticed that velocity profile f' is increased via velocity ratio parameter B. Boundary layer only exist for $B < 1$ and $B > 1$. Impact of magnetic parameter M on velocity f' is sketched in figure 7. Here velocity profile f' declines with increasing values of magnetic parameter M. Physically, for higher magnetic field the resistive force increases and the velocity profile reduces. Due to larger magnetic parameter Lorentz forces are produced that resist the flow of fluid as a result flow of fluid simultaneously reduces.

Figure 8 communicates the vital role of temperature distribution θ via Prandtl number Pr. This figure divulges that by growing Prandtl number Pr, dimensionless distribution θ is maneuvered. Physically by growing the Prandtl number thermal diffusivity reduced as a result temperature of nanoliquid is also diminishes. Figure 9 unveils the inspirations of the temperature ratio parameter θ_f on the temperature field θ. It is obvious that the

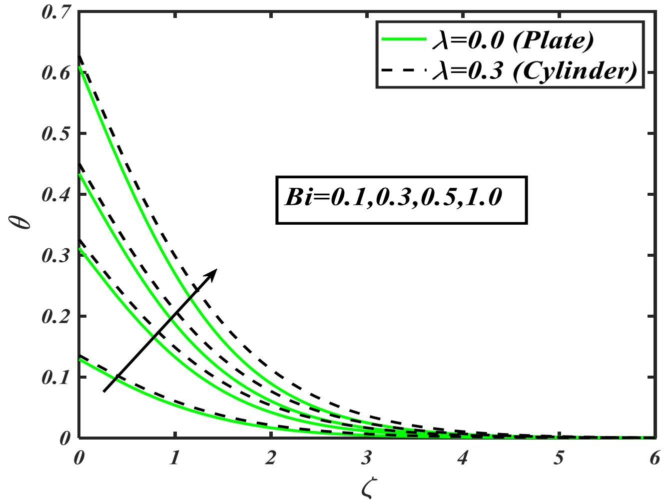

Figure 11. Sketch of θ against Bi.

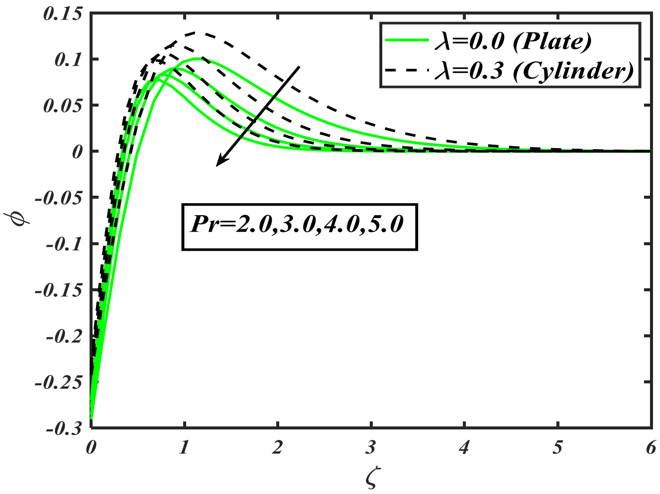

Figure 12. Sketch of ϕ against Pr.

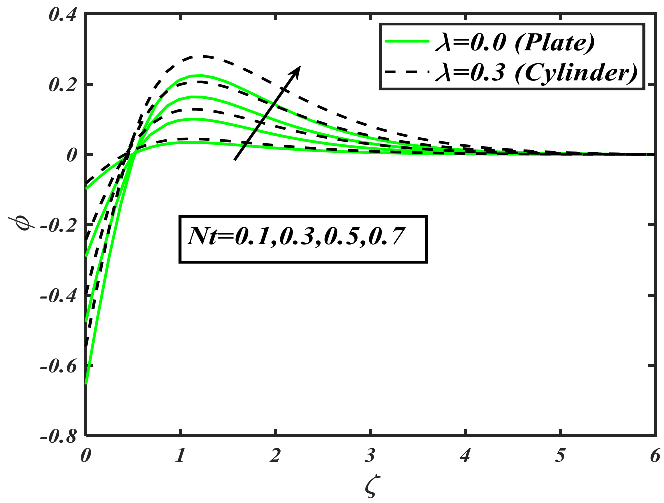

Figure 13. Sketch of ϕ against Nt.

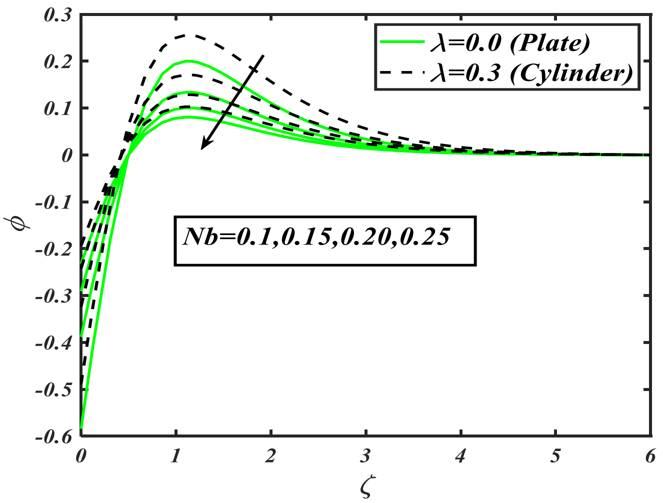

Figure 14. Sketch of ϕ against Nb.

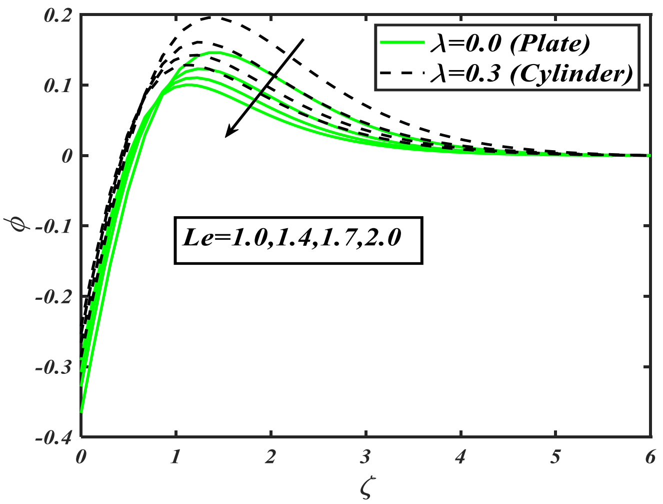

Figure 15. Sketch of ϕ against Le.

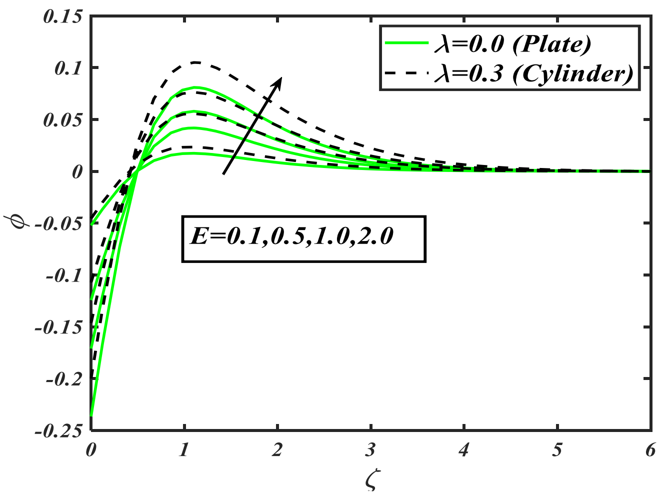

Figure 16. Sketch of ϕ against E.

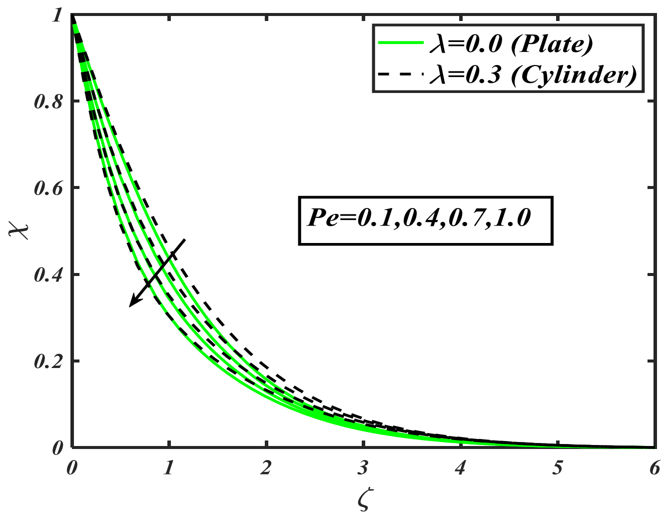

Figure 17. Sketch of χ against Pe.

Table 1. Outcomes of $-f''(0)$ versus M, λ, Nr, Nc, β_1, β_2, B, α.

Parameters								$-f''(0)$	
M	λ	Nr	Nc	β_1	β_2	B	α	$\alpha = 0.0$	$\alpha = 0.3$
0.1	0.2	0.5	0.5	0.3	0.3	0.1	0.1	0.6606	0.8038
0.4								0.7462	0.8826
0.8								0.8421	0.9706
0.5	0.1	0.5	0.5	0.3	0.3	0.1	0.1	0.7621	0.8964
	0.4							0.7917	0.9262
	0.8							0.8333	0.9683
0.5	0.2	0.1	0.5	0.3	0.3	0.1	0.1	0.8422	0.9823
		1.0						0.8230	0.9521
		2.0						0.8049	0.9233
0.5	0.2	0.5	0.1	0.3	0.3	0.1	0.1	0.8782	0.9975
			1.0					0.7194	0.8371
			2.0					0.5618	0.6790
0.5	0.2	0.5	0.5	0.1	0.3	0.1	0.1	0.6064	0.6973
				0.4				0.5419	0.6705
				0.8				0.4769	0.6409
0.5	0.2	0.5	0.5	0.3	0.1	0.1	0.1	0.5729	0.6901
					0.7			0.5400	0.6590
					1.4			0.5038	0.6304
0.5	0.2	0.5	0.5	0.3	0.3	0.3	0.1	0.5493	0.6570
						0.7		0.4830	0.5609
						1.0		0.3821	0.4227
0.5	0.2	0.5	0.5	0.3	0.3	0.1	0.3	0.6054	0.6626
							0.7	0.6344	0.6456
							1.0	0.6654	0.6731

temperature ratio parameter θ_f tends to improve the variation of temperature distribution θ. Figure 10 is delineated to scrutinize the physical aspects of temperature distribution θ over thermophoresis parameter Nt. From the sketched lines of figure that intensification the thermophoresis parameter Nt, put up the temperature field θ. Thermophoresis is a phenomenon in which heated particles are pulled away from warm surface to the cold region. Due to this reality the temperature of the fluid increases. Figure 11 is captured to design the influence of Biot number Bi via distribution profile θ. It is also scrutinized that the temperature field θ enhanced for higher variations of Biot number Bi. Physically Biot number described as intra-particle ratio and external heat transport resistance. Therefore we expect significant intra-particle temperature profiles for high Biot numbers. Figure 12 reveals the effect of the Prandtl number Pr on the volumetric concentration of nano-particles ϕ. The diminishing behavior of volumetric concentration ϕ on enlarging Pr is observed in sketched

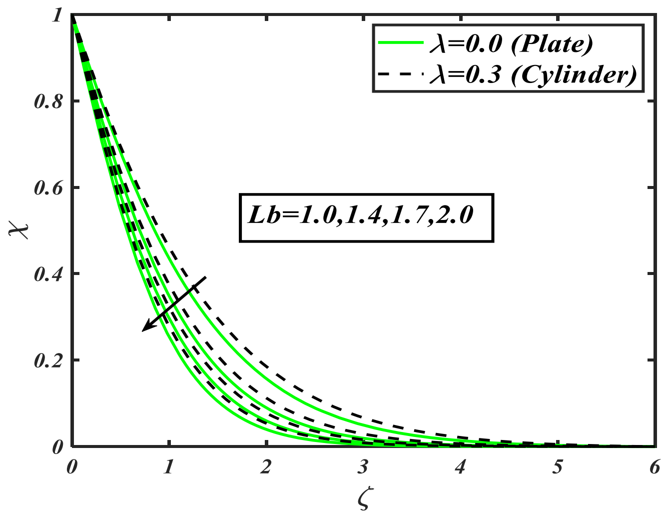

Figure 18. Sketch of χ against Lb.

Table 2. Outcomes of $-\theta'(0)$ versus M, λ, Nr, Nc, β_1, β_2, α, Pr, Nb, Nt, Rd, B,.

Parameters												$-\theta'(0)$	
M	λ	Nr	Nc	β_1	β_2	α	Pr	Nb	Nt	Rd	B	$\alpha = 0.0$	$\alpha = 0.3$
0.1	0.2	0.5	0.5	0.3	0.3	0.1	1.2	0.2	0.3	0.8	2.0	0.3929	0.3769
0.4												0.3801	0.3654
0.8												0.3662	0.3529
0.5	0.1	0.5	0.5	0.3	0.3	0.1	1.2	0.2	0.3	0.8	2.0	0.3777	0.3634
	0.4											0.3635	0.3590
	0.8											0.3571	0.3424
0.5	0.2	0.1	0.5	0.3	0.3	0.1	1.2	0.2	0.3	0.8	2.0	0.3631	0.3475
		1.0										0.3714	0.3579
		2.0										0.3877	0.3669
0.5	0.2	0.5	0.1	0.3	0.3	0.1	1.2	0.2	0.3	0.8	2.0	0.3703	0.3582
			1.0									0.3876	0.3758
			2.0									0.4016	0.3900
0.5	0.2	0.5	0.5	0.1	0.3	0.1	1.2	0.2	0.3	0.8	2.0	0.3987	0.3912
				0.4								0.4031	0.4032
				0.8								0.4183	0.4133
0.5	0.2	0.5	0.5	0.3	0.1	0.1	1.2	0.2	0.3	0.8	2.0	0.4008	0.3883
					0.7							0.4134	0.3931
					1.4							0.4265	0.4080
0.5	0.2	0.5	0.5	0.3	0.3	0.3	1.2	0.2	0.3	0.8	2.0	0.4088	0.3996
						0.7						0.4299	0.4245
						1.0						0.4502	0.4473
0.5	0.2	0.5	0.5	0.3	0.3	0.1	1.0	0.2	0.3	0.8	2.0	0.3672	0.3567
							2.0					0.5064	0.4925
							3.0					0.5936	0.5782
0.5	0.2	0.5	0.5	0.3	0.3	0.1	1.2	0.1	0.3	0.8	2.0	0.4098	0.3998
								0.4				0.3968	0.3841
								0.8				0.3742	0.3609
0.5	0.2	0.5	0.5	0.3	0.3	0.1	1.2	0.2	0.1	0.8	2.0	0.4037	0.3919
									0.4			0.4003	0.3887
									0.8			0.3937	0.3815
0.5	0.2	0.5	0.5	0.3	0.3	0.1	1.2	0.2	0.3	0.1	2.0	0.5088	0.4961
										0.5		0.4401	0.4279
										1.0		0.3803	0.3691
0.5	0.2	0.5	0.5	0.3	0.3	0.1	1.2	0.2	0.3	0.8	1.0	0.5416	0.3285
											1.4	0.5522	0.3611
											1.7	0.5576	0.3776

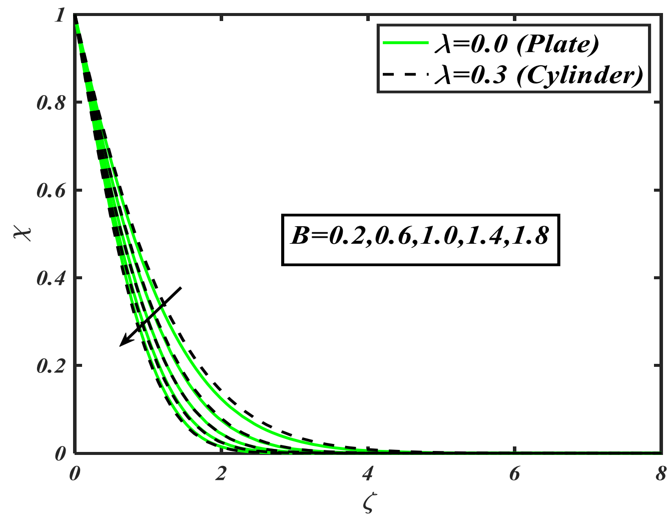

Figure 19. Sketch of χ against B.

Table 3. Outcomes of $-\phi'(0)$ versus M, λ, Nr, Nc, β_1, β_2, α, E, Pr, Nb, Nt, Rd, B,.

Parameters													$-\phi'(0)$	
M	λ	Nr	Nc	β_1	β_2	α	E	Pr	Nb	Nt	Rd	B	$\alpha = 0.0$	$\alpha = 0.3$
0.1	0.2	0.5	0.5	0.3	0.3	0.1	0.1	1.2	0.2	0.3	0.8	2.0	0.5893	0.5653
0.4													0.5701	0.5481
0.8													0.5494	0.5294
0.5	0.1	0.5	0.5	0.3	0.3	0.1	0.1	1.2	0.2	0.3	0.8	2.0	0.5665	0.5451
	0.4												0.5502	0.5386
	0.8												0.5406	0.5267
0.5	0.2	0.1	0.5	0.3	0.3	0.1	0.1	1.2	0.2	0.3	0.8	2.0	0.5446	0.5212
		1.0											0.5571	0.5368
		2.0											0.5682	0.5503
0.5	0.2	0.5	0.1	0.3	0.3	0.1	0.1	1.2	0.2	0.3	0.8	2.0	0.5554	0.5373
			1.0										0.5815	0.5636
			2.0										0.6025	0.5850
0.5	0.2	0.5	0.5	0.1	0.3	0.1	0.1	1.2	0.2	0.3	0.8	2.0	0.5980	0.5850
				0.4									0.6046	0.5959
				0.8									0.6125	0.6023
0.5	0.2	0.5	0.5	0.3	0.1	0.1	0.1	1.2	0.2	0.3	0.8	2.0	0.6011	0.5725
					0.7								0.6151	0.5897
					1.4								0.6298	0.5970
0.5	0.2	0.5	0.5	0.3	0.3	0.3	0.1	1.2	0.2	0.3	0.8	2.0	0.6132	0.5994
						0.7							0.6448	0.6367
						1.0							0.6754	0.6710
0.5	0.2	0.5	0.5	0.3	0.3	0.1	0.4	1.2	0.2	0.3	0.8	2.0	0.6029	0.5848
							0.8						0.6134	0.5931
							1.2						0.6237	0.6064
0.5	0.2	0.5	0.5	0.3	0.3	0.1	0.1	1.0	0.2	0.3	0.8	2.0	0.5508	0.5350
								2.0					0.7596	0.7387
								3.0					0.8903	0.8673
0.5	0.2	0.5	0.5	0.3	0.3	0.1	0.1	1.2	0.1	0.3	0.8	2.0	0.2294	0.1994
									0.4				0.2176	0.1881
									0.8				0.1478	0.1428
0.5	0.2	0.5	0.5	0.3	0.3	0.1	0.1	1.2	0.2	0.1	0.8	2.0	0.9018	0.8959
										0.4			0.8006	0.7773
										0.8			0.5747	0.5262
0.5	0.2	0.5	0.5	0.3	0.3	0.1	0.1	1.2	0.2	0.3	0.1	2.0	0.5088	0.4961
											0.5		0.4401	0.4279
											1.0		0.3803	0.3691
0.5	0.2	0.5	0.5	0.3	0.3	0.1	0.1	1.2	0.2	0.3	0.8	1.0	0.5049	0.4926
												1.4	0.5565	0.5417
												1.7	0.5827	0.5664

Table 4. Outcomes of $-\chi'(0)$ versus M, λ, Nr, Nc, β_1, β_2, α, B, Lb, Pe.

Parameters										$-\chi'(0)$	
M	λ	Nr	Nc	β_1	β_2	α	B	Lb	Pe	$\alpha = 0.0$	$\alpha = 0.3$
0.1	0.2	0.5	0.5	0.3	0.3	0.1	0.2	1.0	0.1	0.6005	0.5706
0.4										0.5801	0.5522
0.8										0.5577	0.5318
0.5	0.1	0.5	0.5	0.3	0.3	0.1	0.2	1.0	0.1	0.5763	0.5489
	0.4									0.5694	0.5318
	0.8									0.5590	0.5210
0.5	0.2	0.1	0.5	0.3	0.3	0.1	0.2	1.0	0.1	0.5529	0.5231
		1.0								0.5658	0.5396
		2.0								0.5773	0.5538
0.5	0.2	0.5	0.1	0.3	0.3	0.1	0.2	1.0	0.1	0.5628	0.5390
			1.0							0.5922	0.5690
			2.0							0.6163	0.5933
0.5	0.2	0.5	0.5	0.1	0.3	0.1	0.2	1.0	0.1	0.6110	0.5930
				0.4						0.6188	0.6035
				0.8						0.6279	0.6142
0.5	0.2	0.5	0.5	0.3	0.1	0.1	0.2	1.0	0.1	0.6048	0.5808
					0.7					0.6194	0.5983
					1.4					0.6247	0.6058
0.5	0.2	0.5	0.5	0.3	0.3	0.3	0.2	1.0	0.1	0.6252	0.6057
						0.7				0.6545	0.6410
						1.0				0.6856	0.6765
0.5	0.2	0.5	0.5	0.3	0.3	0.1	1.0	1.0	0.1	0.6854	0.6132
							1.4			0.6730	0.6346
							1.7			0.6534	0.6418
0.5	0.2	0.5	0.5	0.3	0.3	0.1	0.1	1.2	0.1	0.6867	0.6627
								1.6		0.6135	0.7882
								2.0		0.9268	0.9006
0.5	0.2	0.5	0.5	0.3	0.3	0.1	0.1	1.0	0.2	0.5668	0.5391
									0.6	0.3715	0.3250
									1.0	0.1806	0.1161

lines. The characteristic of nano-particles concentration ϕ and thermophoresis parameter Nt are manifested in figure 13. The curves of concentration field truncate with enhancing variation of thermophoresis parameter. Physically thermophoresis is a phenomenon that moves tiny-particles from hot to cold surfaces. Figure 14 incorporates the consequence of the Brownian motion parameter Nb on the concentration profile ϕ. The volumetric concentration of nano-particles ϕ is dilute with knock up the values of the Brownian motion parameter Nb. Physically a boost in Brownian motion an improvement in the temperature field arises due to the higher haphazard movement of particles.

Figure 15 illustrates the crucial impact of Lewis number Le and nano-particle concentration ϕ. This figure professes that the concentration field ϕ turns down with increment in the values of Lewis number Le. Physically Lewis number is ratio between momentum diffusivity and mass diffusivity. Mass diffusivity rises with enhance in Lewis number, concentration boundary layer reduces. Figure 16 examines the aspects of the activation energy E and volumetric concentration ϕ. As increment in the values of activation energy E, the volumetric concentration ϕ boosted up. Figure 17 is interpreted to examine the behavior of Peclet number Pe on motile microorganism field χ. From this sketched it is analyzed that the motile microorganisms χ reduce for higher values of Peclet number Pe. Figure 18 is scrutinized the physical relation between the bioconvection Lewis number Lb and the rescaled density of motile microorganism's field χ. An interesting behavior observed, by augmentation of the bioconvection Lewis number Lb, motile microorganism's concentration χ decline. Figure 19 illustrates the impact of velocity ratio parameter B against motile microorganism concentration χ. From this scenario, It is noticed the microorganism concentration χ decrease for higher values of velocity ratio parameter B.

Table 1 is constructed for characteristics of involves parameters such as, magnetic parameter, mixed convection parameter, buoyancy ratio parameter, third grade parameter, velocity ratio parameter, and activation energy M, λ, Nr, Nc, β_1, β_2, B, α respectively on skin fraction coefficient increases for β_1, λ, Nr, M, Nc, but opposite impact is observed against β_2, and B. Table 2 is captured to examine the salient behavior of involved parameter against local Nusselt number. It is noticed that, local Nusselt number upsurges for Nr, Nc, β_1, B. The significance of local Sherwood number versus involved parameter is depicted in table 3. The local Nusselt number is decreasing function for Brownian motion and thermophoresis parameter while opposite trend for β_1, β_2. The features of involved parameters over local density number of motile microorganism are shown in table 4. The local density number motile microorganism are reduces for higher values of *Pe* and *Lb*.

5. Conclusions

The salient features of bioconvection in the stagnation point flow of third grade fluid across a radiative stretching cylinder considering motile microorganisms are studied. Velocity profile increases for higher mixed convection parameter. Prandtl number has a similar behavior on temperature distribution and concentration of nanoparticles [48, 49]. The significance of thermophoresis parameter on volumetric nanoparticles concentration and temperature distribution are dissimilar in nature. Density of motile microorganism concentration lessens with growing Peclet number and bio-convection Lewis number.

Acknowledgements

The authors extend their appreciation to the Deanship of Scientific Research at King Khalid University, Abha, Saudi Arabia for funding this work through general research groups program under grant number G.R.P-150/42.

ORCID iDs

Hassan Waqas https://orcid.org/0000-0002-0388-8506
Arshad Riaz https://orcid.org/0000-0003-0717-6677

References

[1] Choi S U S 1995 Enhancing thermal conductivity of fluid with Nanoparticles developmentsan applications of non-Newtonian flow *ASME FED* **66** 99–105
[2] Buongiorno J 2006 Convective transport in Nanofluids *J. Heat Transfer* **128** 240–50
[3] Alamri S Z, Khan A A, Azeez M and Ellahi R 2019 Effects of mass transfer on MHD second grade fluid towards stretching cylinder: a novel perspective of Cattaneo-Christov heat flux model *Phys. Lett.* A **383** 276–81
[4] Khan M I, Alzahrani F, Hobiny A and Ali Z 2020 Fully developed second order velocity slip Darcy-Forchheimer flow by a variable thicked surface of disk with entropy generation *Int. Commun. Heat Mass Transfer* **117** 104778
[5] Abbas S Z, Khan M I, Kadry S, Khan W A, Israr-Ur-Rehman M and Waqas M 2020 Fully developed entropy optimized second order velocity slip MHD nanofluid flow with activation energy *Comput. Methods Programs Biomed.* **190** 105362
[6] Wang J, Khan M I, Khan W A, Abbas S Z and Khan M I 2020 Transportation of heat generation/absorption and radiative heat flux in homogeneous–heterogeneous catalytic reactions of non-Newtonian fluid (Oldroyd-B model) *Comput. Methods Programs Biomed.* **189** 105310
[7] Muhammad R, Khan M I, Khan N B and Jameel M 2020 Magnetohydrodynamics (MHD) radiated nanomaterial viscous material flow by a curved surface with second order slip and entropy generation *Comput. Methods Programs Biomed.* **189** 105294
[8] Khan M I, Waqas M, Hayat T and Alsaedi A 2017 A comparative study of Casson fluid with homogeneous-heterogeneous reactions *J. Colloid Interface Sci.* **498** 85–90
[9] Khan M I and Alzahrani F 2020 Binary chemical reaction with activation energy in dissipative flow of non-Newtonian nanomaterials *Journal of Theoretical and Computational Chemistry* **19** 2040006
[10] Hayat T, Khan M I, Farooq M, Alsaedi A, Waqas M and Yasmeen T 2016 Impact of Cattaneo–Christov heat flux model in flow of variable thermal conductivity fluid over a variable thicked surface *Int. J. Heat Mass Transfer* **99** 702–10
[11] Hosseini S R, Ghasemian M, Sheikholeslami M, Shafee A and Li Z 2019 Entropy analysis of nanofluid convection in a heated porous micro channel under MHD field considering solid heat generation *Powder Tech.* **344** 914–25
[12] Waqas M, Jabeen S, Hayat T, Khan M I and Alsaedi A 2019 Modeling and analysis for magnetic dipole impact in nonlinear thermally radiating Carreau nanofluid flow subject to heat generation *J. Magn. Magn. Mater.* **485** 197–204
[13] Ashlin T S and Mahanthesh B 2019 Exact solution of non-coaxial rotating and non-linear convective flow of Cu–Al_2O_3–H_2O hybrid Nanofluids over an infinite vertical plate subjected to heat source and radiative heat *J. Nanofluids* **8** 781–94
[14] Khan M I, Qayyum S, Kadry S, Khan W A and Abbas S Z 2020 Theoretical investigations of entropy optimization in electro-magneto nonlinear mixed convective second order slip flow *Journal of Magnetics* **25** 8–14
[15] Ali A, Mumraiz S, Nawaz S, Awais M and Asghar S 2020 Third grade fluid flow of stretching cylinder with heat source/sink *Journal of Applied and Computational Mechanics* **6** 1125–32
[16] Hayat T, Riaz R, Aziz A and Alsaedi A 2020 Influence of Arrhenius activation energy in MHD flow of third grade nanofluid over a nonlinear stretching surface with convective heat and mass conditions *Physica* A **549** 124006
[17] Chaudhuri S and Kumar Rathore S 2019 Semi analytical solution of heat transfer of magnetohydrodynamic third-grade fluids flowing through parallel plates with viscous dissipation *Journal of Thermal Science and Engineering Applications* **11** 024504
[18] Hayat T, Riaz R, Aziz A and Alsaedi A 2019 Analysis of entropy generation for MHD flow of third grade nanofluid over a nonlinear stretching surface embedded in a porous medium *Phys. Scr.* **94** 125703
[19] Alzahrani E O, Shah Z, Dawar A and Malebary S J 2019 Hydromagnetic mixed convective third grade nanomaterial containing gyrotactic microorganisms toward a horizontal stretched surface *Alexandria Engineering Journal* **58** 1421–9

[20] Okoya S S 2019 Computational study of thermal influence in axial annular flow of a reactive third grade fluid with non-linear viscosity *Alexandria Engineering Journal* **58** 401–11

[21] Sajid M, Mughees M, Ali N and Shahzad H 2019 A theoretical analysis of blade coating for third-grade fluid *Journal of Plastic Film & Sheeting* **35** 218–38

[22] Mahanthesh B and Joseph T V 2019 Dynamics of magneto-nano third-grade fluid with Brownian motion and thermophoresis effects in the pressure type die *Journal of Nanofluids* **8** 870–5

[23] Golafshan B and Rahimi A B 2019 Effects of radiation on mixed convection stagnation-point flow of MHD third-grade nanofluid over a vertical stretching sheet *J. Therm. Anal. Calorim.* **135** 533–49

[24] Hiemenz K and Grenzschicht D 1911 an einem in den gleich formigen Flussig keits stromeingetauchtengeradenKreiszylinder *Dinglers Polytech. J.* **326** 321–4

[25] Saif R S, Hayat T, Ellahi R, Muhammad T and Alsaedi A 2017 Stagnation-point flow of second grade nanofluid towards a nonlinear stretching surface with variable thickness *Results in Physics* **7** 2821–30

[26] Ghasemian A, SaeedDinarvand, ArmenAdamian and Sheremet M A 2019 Unsteady general three-dimensional stagnation point flow of a maxwell/buongiorno non-newtonian nanofluid *Journal of Nanofluids* **8** 1544–59

[27] Khan W A, Rashad A M, Abdou M M M and Tlili I 2019 Natural bioconvection flow of a nanofluid containing gyrotatic microorganisms about a truncated cone *European Journal of Mechanics-B/Fluids* **75** 133–42

[28] Rashad A M and Nabwey H A 2019 Gyrotactic mixed bioconvection flow of a nanofluid past a circular cylinder with convective boundary condition *J. Taiwan Inst. Chem. Eng.* **99** 9–17

[29] Naz R, Noor M, Hayat T, Javed M and Alsaedi A 2020 Dynamism of magnetohydrodynamic cross nanofluid with particulars of entropy generation and gyrotactic motile microorganisms *Int. Commun. Heat Mass Transfer* **110** 104431

[30] Al-Khaled K, Khan S U and Khan I 2020 Chemically reactive bioconvection flow of tangent hyperbolic nanoliquid with gyrotactic microorganisms and nonlinear thermal radiation *Heliyon* **6** e03117

[31] Waqas H, Khan S U, Tlili I, Awais M and Shadloo M S 2020 Significance of bioconvective and thermally dissipation flow of viscoelastic nanoparticles with activation energy features: novel biofuels significance *Symmetry* **12** 214

[32] Balla C S, Alluguvelli R, Naikoti K and Makinde O D 2020 Effect of chemical reaction on bioconvective flow in oxytactic microorganisms suspended porous cavity *Journal of Applied and Computational Mechanics* **6** 653–64

[33] Naganthran K, Basir M F M, Kasihmuddin M S M, Ahmed S E, Olumide F B and Nazar R 2020 Exploration of dilatant nanofluid effects conveying microorganism utilizing scaling group analysis: FDM Blottner *Physica A* **549** 124040

[34] Zuhra S, Khan N S, Alam M, Islam S and Khan A 2020 Buoyancy effects on nanoliquids film flow through a porous medium with gyrotactic microorganisms and cubic autocatalysis chemical reaction *Advances in Mechanical Engineering* **12** 1687814019897510

[35] Mansour M A, Rashad A M, Mallikarjuna B, Hussein A K, Aichouni M and Kolsi L 2019 MHD mixed bioconvection in a square porous cavity filled by gyrotactic microorganisms *Int. J. Heat Technol.* **37** 433–45

[36] Zeng L and Pedley T J 2018 Distribution of gyrotactic micro-organisms in complex three-dimensional flows. Part 1. Horizontal shear flow past a vertical circular cylinder *J. Fluid Mech.* **852** 358–97

[37] Khan M, Salahuddin T, Malik M Y and Alqarni M S 2020 Numerical modelling and analysis of bioconvection on MHD flow due to an upper paraboloid surface of revolution *Physica A* **553** 124231

[38] Mallikarjuna B, Rashad A M, Chamkha A and Abdou M M M 2018 Mixed bioconvection flow of a nanofluid containing gyrotactic microorganisms past a vertical slender cylinder *Frontiers in Heat and Mass Transfer (FHMT)* **10** 21

[39] Waqas H, Khan S U, Hassan M, Bhatti M M and Imran M 2019 Analysis on the bioconvection flow of modified second-grade nanofluid containing gyrotactic microorganisms and nanoparticles *J. Mol. Liq.* **291** 111231

[40] Waqas H, Khan S U, Imran M and Bhatti M M 2019 Thermally developed Falkner–Skanbioconvection flow of a magnetized nanofluid in the presence of a motile gyrotactic microorganism: Buongiorno'snanofluid model *PhysicaScripta* **94** 115304

[41] Khan S U, Waqas H, Bhatti M M and Imran M 2020 Bioconvection in the rheology of magnetized couple stress nanofluid featuring activation energy and Wu's Slip *J. Non-Equilib. Thermodyn.* **45** 81–95

[42] Ray A K, Vasu B, Beg O A, Gorla R S R and Murthy P V S N 2019 Magneto-bioconvection flow of a Casson thin film with nanoparticles over an unsteady stretching sheet *Int. J. Numer. Methods Heat Fluid Flow* **29** 4277–309

[43] Amirsom N A, Uddin M J, Basir M F M, Ismail A, Beg O A and Kadir A 2019 Three-dimensional bioconvectionnanofluid flow from a bi-axial stretching sheet with anisotropic slip *Sains Malaysiana* **48** 1137–49

[44] Khan M I, Haq F, Khan S A, Hayat T and Khan M I 2020 Development of thixotropic nanomaterial in fluid flow with gyrotactic microorganisms, activation energy, mixed convection *Comput. Methods Programs Biomed.* **187** 105186

[45] Naz R, Tariq S and Alsulami H 2020 Inquiry of entropy generation in stratified Walters' B nanofluid with swimming gyrotactic microorganisms *Alexandria Engineering Journal* (https://doi.org/10.1016/j.aej.2019.12.037)

[46] Chakraborty T, Das K and Kundu P K 2018 Framing the impact of external magnetic field on bioconvection of a nanofluid flow containing gyrotactic microorganisms with convective boundary conditions *Alexandria Engineering Journal* **57** 61–71

[47] Khan M I, Alzahrani F and Hobiny A 2020 Heat transport and nonlinear mixed convective nanomaterial slip flow of Walter-B fluid containing gyrotactic microorganisms *Alexandria Engineering Journal*

[48] Riaz A, Zeeshan A, Bhatti M M and Ellahi R 2020 Peristaltic propulsion of Jeffrey nano-liquid and heat transfer through a symmetrical duct with moving walls in a porous medium *Physica A* **545** 123788

[49] Alolaiyan H, Riaz A, Razaq A, Saleem N, Zeeshan A and Bhatti M M 2020 Effects of double diffusion convection on third grade nanofluid through a curved compliant peristaltic channel *Coatings* **10** 154